PNAS RESEARCH ARTICLE | EARTH, ATMOSPHERIC, AND PLANETARY SCIENCES OPEN ACCESS

Carbonate burial regimes, the Meso-Cenozoic climate, and nannoplankton expansion

Tristan Salles[a,1,2], Laurent Husson[b,1], Thran Trung Nguyen[a,c], Ana Vila-Concejo[a,c], Jonathon Leonard[a], Ana Paula Da Silva[a,c], Jody M. Webster[a,c], and Fabienne Giraud[b]

Affiliations are included on p. 9.

Edited by Lee Kump, The Pennsylvania State University, University Park, PA; received June 27, 2025; accepted November 6, 2025

The long-term climate of Earth alternates between warmer and cooler periods, for which atmospheric CO_2 content is often viewed as a primary control. Although silicate weathering feedback governs this long-term equilibrium, the partitioning of carbonate burial between neritic and pelagic environments can influence how rapidly the carbon cycle adjusts to perturbations. The impact of neritic carbonates accumulation on oceanic calcium and alkalinity fluxes, nannoplankton productivity, and carbon reservoirs is overlooked. To investigate this role, we combine plate-tectonic reconstructions with climatic and physiographic simulations and apply a macroecological model to estimate Meso-Cenozoic neritic warm-water carbonate habitats and productivity. We find that only during the Early Cretaceous and Cenozoic did geochemical influxes exceed the carbonate accumulation potential of neritic platforms, while for most of the interval they fell short. These alternating states define two regimes: i) habitability-limited periods, where environmental conditions restrict the development of neritic carbonate factories, and ii) alkalinity-limited periods, where ocean chemistry restricts carbonate precipitation. By alternating between these regimes, neritic platforms modulate the buffering capacity and the timescales (10^3 to 10^5 years) of carbon cycle recovery and regulate the development and productivity of nannoplankton, and therefore the biological pump. This framework highlights the role of shallow-water carbonate systems as important modulators of the Earth's climate system and pelagic ecosystems.

carbonate productivity | species distribution model | paleo-climate

Significance

Shallow-water carbonate platforms, home to ecosystems like coral reefs, play a crucial but underappreciated role in modulating Earth's carbon cycle. By integrating plate tectonic, climate, and ecological models, we reconstruct global patterns of carbonate productivity over the past 265 My. We identify alternating regimes in which carbonate deposition is limited by habitat space or by chemical supply, influencing the timescales over which the carbon cycle responds to perturbations. This neritic-pelagic partitioning modulates carbon cycle buffering and recovery, rather than serving as the primary control of long-term atmospheric CO_2, which is ultimately governed by silicate weathering feedback. Our results offer a perspective on the interplay between climate evolution, ocean chemistry, and marine biodiversity through deep time.

While the silicate-weathering feedback sets the long-term equilibrium of atmospheric CO_2 (1–3), other components of the carbon cycle influence how rapidly the system adjusts to perturbations. In particular, the capacity of the oceans to precipitate and sequester calcium carbonates contributes to buffering climate variability. Cenozoic cooling, for example, has been associated with an increase in deep-sea carbonate deposition, driven by interactions between Ca^{2+} and HCO_3^- fluxes, pelagic carbonate accumulation, and changes in atmospheric CO_2 levels (4–6). These processes collectively influenced long-term climate trends.

Here, we hypothesize that over millions of years, the accumulation of shallow-water carbonates can influence the partitioning of calcium and carbonate ions between neritic and pelagic reservoirs. By trapping these ions in shallow environments, neritic carbonates reduce deep-sea burial and alter the buffering capacity of the oceans, thus modulating the timescales (10^3 to 10^5 y) over which the carbon cycle recovers from perturbations. This dynamic system is well exemplified by the fluctuating depth of carbonate accumulation due to changes in both ocean chemistry and the balance between neritic and pelagic burial (7). We frame this effect in terms of two contrasted regimes: i) habitability-limited periods, where environmental constraints restrict carbonate factory development, and ii) alkalinity-limited periods, where ocean chemistry constrains carbonate precipitation. This two-regime perspective provides a framework for linking the dynamics of climate evolution to neritic carbonate productivity (although additional processes interact with this partitioning). The efficiency of the biological pump and variations in the burial of organic carbon can strongly influence atmospheric CO_2, particularly during periods of widespread anoxia (8, 9). In the long-term, the biological pump should also depend on the productivity capacity of pelagic nannoplanktonic life, the evolution of which is itself contingent on partitioning of chemical fluxes between neritic and pelagic reservoirs.

To test our hypothesis, we quantify the long-term accumulation of warm-water neritic carbonates (10, 11), which include both tropical carbonate shelves and isolated rimmed

The authors declare no competing interest.

This article is a PNAS Direct Submission.

[1]T.S. and L.H. contributed equally to this work.

[2]To whom correspondence may be addressed. Email: tristan.salles@sydney.edu.au.

This article contains supporting information online at https://www.pnas.org/lookup/suppl/doi:10.1073/pnas.2516468122/-/DCSupplemental.

Published December 4, 2025.

platforms [collectively referred to as the photozoan-T carbonate factory (12, 13)]. In the modern ocean, warm-water carbonates are mostly confined to the intertropical zone, but their spatial distribution has fluctuated over time (14–16) as paleogeography, plate tectonics, and paleoclimatic conditions have changed (17). Although general concepts and broad evolutionary trends have been identified (14, 18, 19), reconstructing the dynamics of the carbonate system remains challenging (20, 21) due to the incompleteness of the geological record, sampling heterogeneity, and the complexity of biotic and abiotic associations (15).

To address these limitations, we used recently published paleogeographic (22), paleoclimatic (23), and paleophysiographic (24) datasets to drive a macroecological model (25) and reconstruct past carbonate factories. Species distribution models (SDM) have proven to be effective tools to describe the relationships between physical environments and life, as well as to predict the impacts of environmental changes on marine organisms (26, 27). Here, we extend this approach to deep time by applying the modern environmental tolerances of warm-water carbonates to ancient conditions, thereby quantifying their productivity potential over time (*SI Appendix*, Fig. S1). We begin by empirically analyzing the environmental niches of warm-water carbonates. We then used these results to infer past potential habitats from paleoenvironmental reconstructions. Next, we benchmark our predictions against the fossil record. We then calculated the shallow-water carbonate productivity potential through time, constraining it with environmental factors and fluvial and hydrothermal chemical fluxes, and compared our results with independent observations and models. Finally, we convert these estimates into Meso-Cenozoic carbonate productivity curves and compare them to the Meso-Cenozoic climate and nannoplanktonic diversification trends, which, we hypothesize, also depend on calcium concentration and alkalinity as well as evolutionary innovations that enhanced pelagic calcification capacity (e.g., the rise of coccolithophores in the Late Cenozoic), themselves also dependent on the chemical concentration of pelagic reservoirs. Our results show that neritic carbonates, although not primary regulators of atmospheric CO_2, were important modulators of buffering capacity, nutrient fluxes, and recovery timescales within the Earth system.

Shifts in Warm-Water Carbonate Habitability

To evaluate the habitability-limited regime, we first reconstruct how the distribution of suitable environments for neritic carbonate production evolved through time in response to tectonic and climatic forcing. Past latitudinal shifts in habitat are often interpreted as responses to changing climatic conditions (10, 15, 27, 28). However, plate tectonics also plays a crucial role in shaping the geomorphology of continental shelves (22), thereby regulating the availability of suitable habitats for neritic carbonate communities (27) and influencing patterns of marine biodiversity (19). Fossil records, lithofacies maps, paleogeography, and plate reconstructions suggest that warm-water carbonates were less tightly confined to the tropics in the geological past than they are today (15). However, fossil databases (29) are strongly biased by the uneven nature of the record (30) and by preferential sampling in the Northern Hemisphere (16). These biases limit the ability to robustly correlate carbonate paleodistributions with abiotic factors across space and time (16, 27, 31). To overcome these limitations, we applied a modeling framework that integrates paleogeographic, climatic, and physiographic reconstructions. Specifically, we use the BIOMOD2 metamodel (25), first to infer the modern environmental suitability of warm-water carbonates with respect to key environmental predictors (sea surface salinity and temperature, bathymetry, large-scale oceanic circulation, terrigenous flux, and ocean surface currents), and second to project this habitat suitability over the past 265 My (Fig. 1 and *SI Appendix*, Fig. S2).

The ensemble model reveals that environmentally suitable habitats for warm-water carbonates were largely concentrated in the Northern Hemisphere—particularly between 5° and 20°N—throughout much of the Mesozoic and early Cenozoic (Fig. 2*A* and *SI Appendix*, Fig. S3). This modeled distribution is independent of sampling biases in the reef fossil record but is regardless consistent with the geographic distribution of fossil occurrences (Fig. 2) which is indeed unevenly distributed toward the Northern Hemisphere. To track long-term trends, we calculate the centroid of predicted suitable habitats, defined here as the average latitude of all suitable areas. This provides a simple measure of whether habitats are preferentially concentrated in tropical or subtropical belts. More broadly, during the Mesozoic, the centroids (Fig. 2*B*) repeatedly shifted between the tropical and subtropical zones, indicating reorganizations of the carbonate-producing regions (27) contingent on continental drift and climatic changes (32). During the Late Permian and Middle Triassic, continental drift shifted suitable habitats from subtropical to higher northern latitudes (10° to 30°N), reducing low-latitude shallow habitats in the Southern Hemisphere.

Modest latitudinal expansions occurred during the Late Jurassic and Late Cretaceous, when warm-water carbonate habitability reached its maximum extent (*SI Appendix*, Fig. S3). This expansion was driven by the combined effects of the rise in sea level—which increased the shelf area (33)—and elevated sea surface temperatures (34, 35) (*SI Appendix*, Fig. S4 *A* and *C*). At the Jurassic-Cretaceous boundary, suitable habitats decreased substantially due to a major fall in global sea level (33), probably related to brief cooling events and potential polar ice development (34, 36) (Fig. 2*A*). The Cretaceous thermal optimum, evident in both fossil records and inferred carbonate production maxima (15) (*SI Appendix*, Table S1), is exemplified by expansive carbonate platforms in the Mediterranean Tethys, North America, Russia, and Siberia (37), and extensive rudist-dominated buildups on Pacific oceanic rises (38). The Cenozoic marks a general contraction of habitable areas toward the tropics and subtropics and a decline in habitat density, coinciding with falling sea surface temperatures (35, 39), lower sea levels, and the replacement of broad passive margins by narrow active ones. This trend includes a pole-to-equator shift in suitable habitat centroids during the Paleocene, reflecting the increasing dominance of tropical environments as temperate regions cooled.

These changes support the hypothesis that the modern latitudinal biodiversity gradient emerged in the late Paleogene with the onset of cooler icehouse conditions (19, 40). Shifts in continental configuration further contributed to this transition: the equatorward movement of the Australian Plate and its convergence with the Eurasian and Philippine plates (41) expanded shallow tropical marine habitats, forming biodiversity hotspots such as the Indo-Australian Archipelago (19, 41) and promoting the tropical concentration of reefal biota (42). Together, these results suggest that steep latitudinal biodiversity gradients became established from the late Paleogene onward (Fig. 2*A*), while flatter gradients characterized the Mesozoic and early Paleogene (27). Although hemispheric habitat centroids generally mirror each other over the Meso-Cenozoic, the northern centroid remains

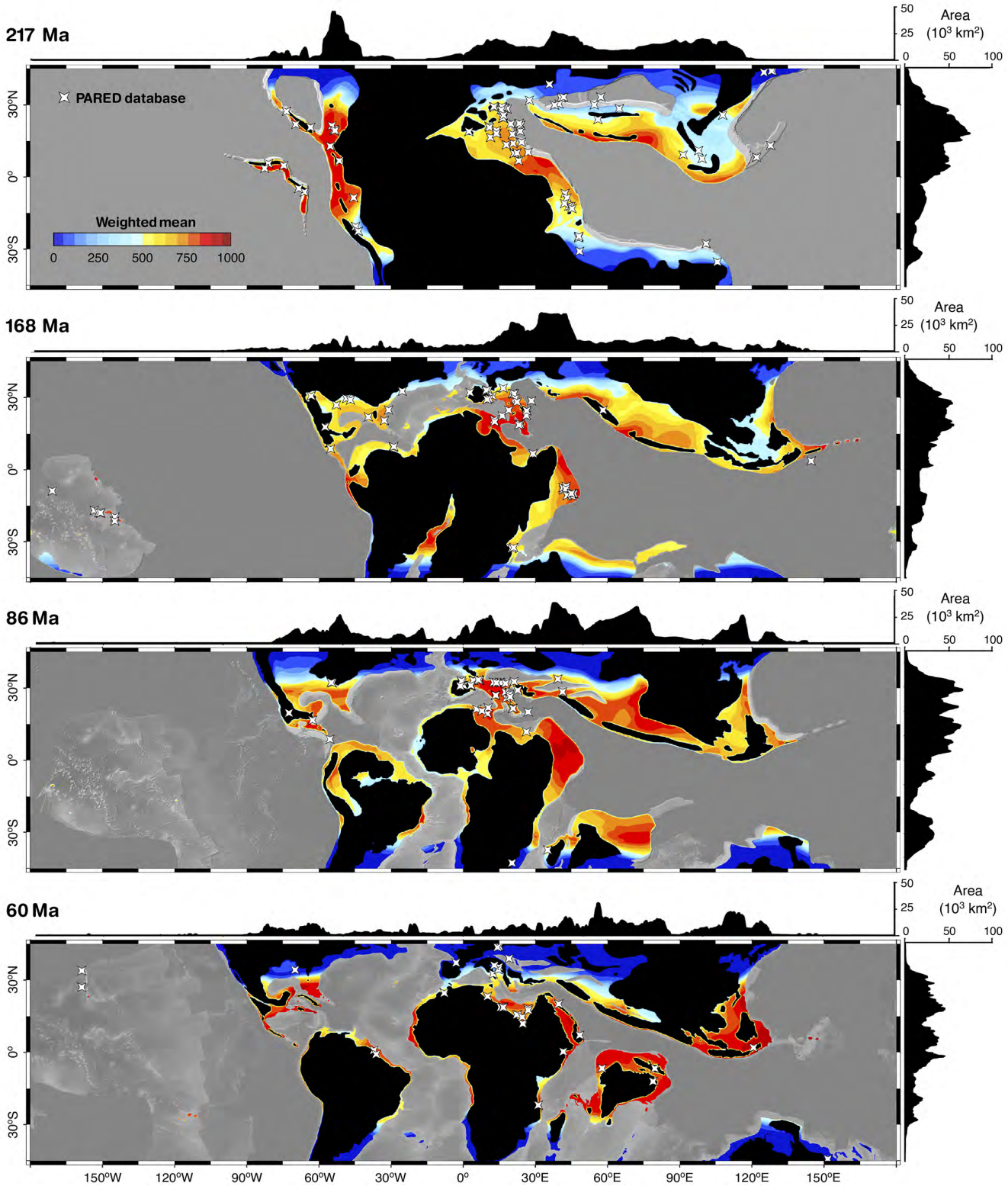

Fig. 1. Modeling the warm-water carbonate habitability across time. Snapshots of the geographical distribution since the Triassic from macroecological ensemble models [species distribution modeling (25)]. Distribution maps of suitable habitats are weighted by ensemble model agreement. Paleontological observations of ancient reefs [white stars, PaleoReef Database PARED (29)] of given geological ages were spatially migrated to their ancient locations, within the limits of their positions on shelves based on paleo-coastlines and continental flooding reconstructions (22). Latitudinally and longitudinally integrated areas of habitable regions (0.5° bins) are shown above and to the right of each map.

more stable, while the southern centroid oscillates (Fig. 2*B*). These shifts predominantly reflect the expansion and contraction of continental shelves (22, 27), and are largely decoupled from atmospheric pCO_2 levels, as the latitudinal drifts of habitat suitability centroids remain similar across alternative pCO_2 scenarios (Fig. 2*B* and *SI Appendix*, Fig. S4*B*). Last, the latitudinal

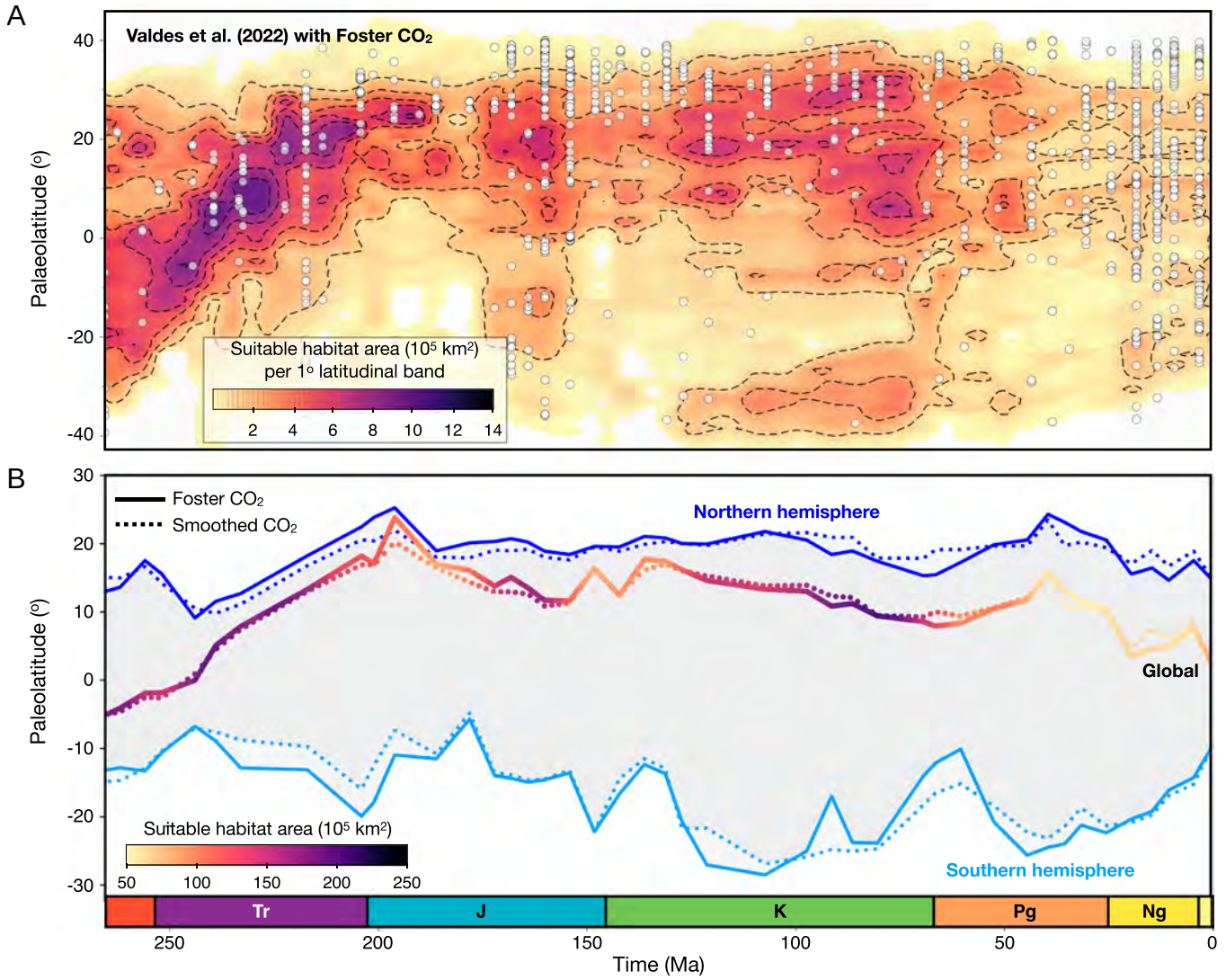

Fig. 2. Latitudinal and temporal evolution in warm-water carbonate habitability over the Meso-Cenozoic [species distribution ensemble model (25)]. (*A*) Paleolatitudinal (1° bins) estimates of environmentally suitable habitat area, based on plate tectonic and bathymetric and climatic reconstructions (23) [based on Foster et al. (39) pCO_2 reconstruction, see *SI Appendix* for an alternative, smoothed-pCO_2 scenario (23)]. Paleontological observations of ancient reefs [white circles, PaleoReef Database (PARED) (29)] were spatially migrated to their ancient latitudes and grouped by geological stages. Isocontours of suitable habitat areas (dashed lines) are given every 200,000 km^2. (*B*) Paleolatitudinal shifts in the centroids of suitable habitats for warm-water carbonates under two pCO_2 scenarios [Foster et al. (39) and smoothed CO_2 (23)]. Paleolatitudinal shifts in the centroid of suitable habitats are first calculated globally and curves for each pCO_2 scenario are color-coded based on suitable habitat areas. The centroid represent the mean paleolatitude of suitable habitat area. The centroids are also computed for each hemisphere based on northern (navy blue) and southern (light blue) suitable habitat areas. All the centroids calculations are carried out with weights proportional to the area of each suitable cell to account for variable cell area with latitude. Triassic (Tr), Jurassic (J), Cretaceous (K), Paleogene (Pg), and Neogene (Ng).

distribution of predicted suitable habitats aligns well with known fossil occurrences (29) (Fig. 2*A*), validating our approach for producing a continuous, quantitative reconstruction of the warm-water carbonate distribution over time.

The spatial integration of habitable regions yields a measure of the cumulated suitable area at any given time, which reaches a maximum extent during the Triassic, Late Jurassic, and Late Cretaceous periods and which declines more than twofold in the intervening periods (magenta line in Fig. 3*A*). Overall, these predicted trends are consistent with available model estimates of neritic carbonate deposition and tropical coral reef development, including probabilistic approaches (27, 43) and physical models (37) (Fig. 3*A*). This agreement is particularly strong for the Cretaceous, where a plateau during the Aptian–Albian interval (115 to 100 Ma) is followed by a nearly continuous rise that culminates in a peak during the Campanian (80 Ma). Discrepancies in magnitude compared to Jones et al. (27) likely arise from its coarser spatial resolution and simplified environmental predictors.

However, the general agreement between models is challenged by geological observations. While the modeled peak in Late Cretaceous warm-water carbonate habitability and the subsequent Cenozoic decline align with trends derived from paleogeographic lithofacies analyses (15, 44) (Fig. 3*A*), this congruence weakens for earlier intervals. In deeper times, model-predicted habitability increasingly exceeds what is observed in the geological record, which does not show the modeled peaks during the Triassic and Jurassic. We suggest that these discrepancies reflect preservation biases rather than model failure. To test this hypothesis and validate our estimates, we compute the loss of carbonate units

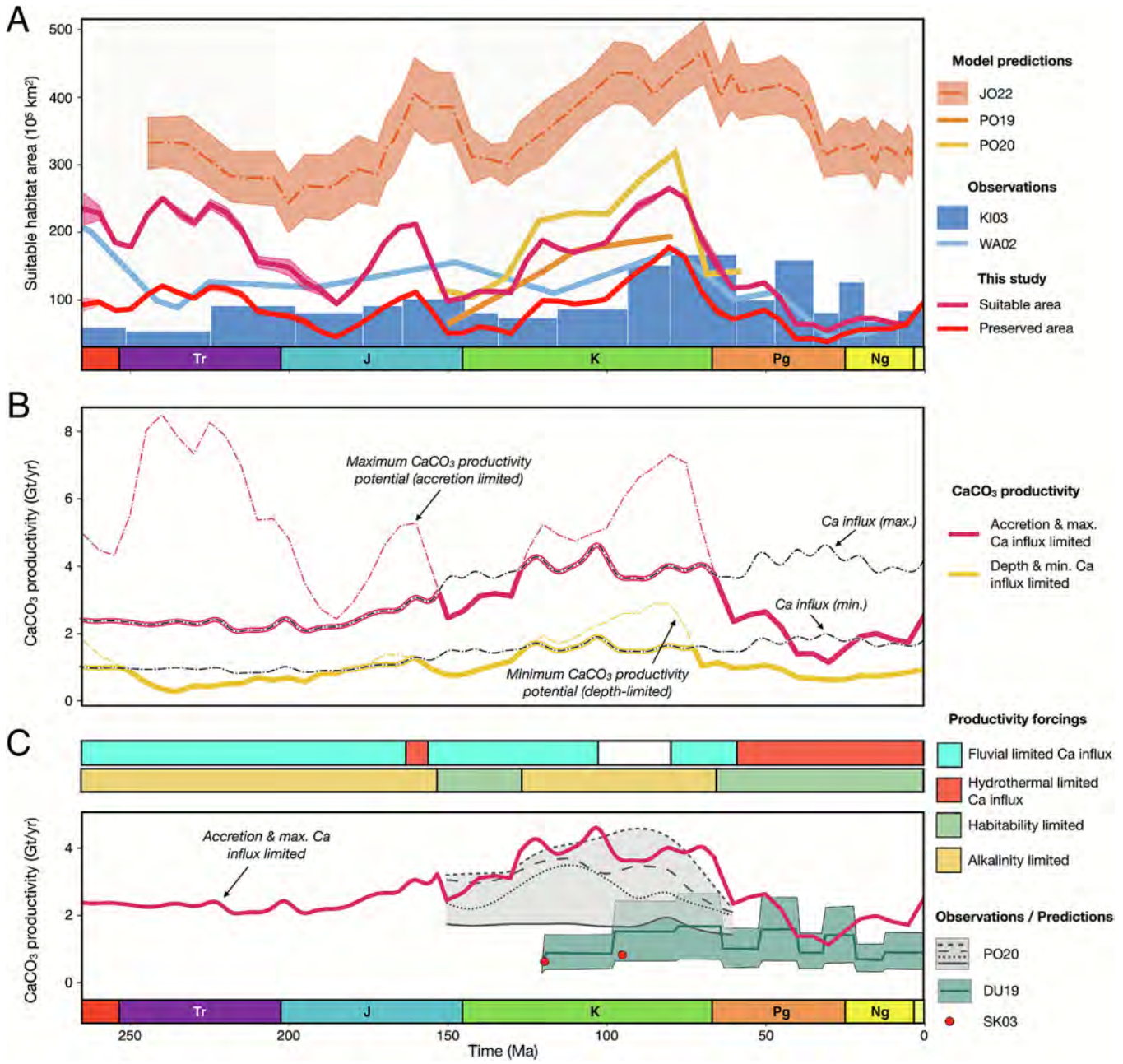

Fig. 3. Warm-water carbonates habitability and productivity. (*A*) Model-predicted suitable habitat area at corresponding time intervals (total, magenta) and preserved at present-day [reconstructed using PALEOMAP plate model (45), red]. Alternative model predictions are provided for comparison: JO22 is modeled using Maxent algorithm (27); PO19 models Cretaceous carbonate platforms area based on fuzzy logic (43); PO20 corresponds to shallow-marine areas available to neritic Cretaceous carbonate deposition (37). The two other trends [KI03 (15) and WA02 (44)] are derived from paleogeographical lithofacies analysis. (*B*) Maximum productivity potential (thin dash-dotted magenta curve) from modeled suitable habitat area (magenta curve, panel *A*); Actual productivity (thick magenta curve), constrained by maximum Ca^{2+} and HCO_3^- influx from hydrothermal, riverine, and groundwater sources (black dash-dotted curve). (*C*) Comparison of carbonate productivity (maximum accumulation rate limited by maximum calcium influx) to alternative model predictions (PO20) (37) and observations [DU19 (5), SK03 (52)]. Triassic (Tr), Jurassic (J), Cretaceous (K), Paleogene (Pg), and Neogene (Ng).

due to subduction by reconstructing the fraction of model-predicted units preserved at present-day [using PALEOMAP plate model (45), *SI Appendix*, Fig. S5]. As expected, preservation declines with age: more than 50% of Triassic and Jurassic units are lost by today. Additional loss may result from chemical and physical weathering (46), while tectonic burial in foreland basins and fold-and-thrust belts can conversely enhance preservation by shielding carbonate units from erosion. These processes are expected to represent only a minor effect and are not considered in our model. At present-day, preserved predicted suitable areas substantially overlap with known Mesozoic carbonate outcrops—particularly in the Northern Hemisphere (29, 47)—and correspond to Cenozoic carbonate-rich stratigraphic sequences (48) (*SI Appendix*, Fig. S5*B*). When we compare the preserved predicted areas with lithofacies-based estimates (15, 44), we find good agreement in both trend and magnitude (red line in Fig. 3*A*), albeit for contrasting reasons. For instance, the Late Cretaceous-Early Paleogene maximum reflects a true peak in warm-water carbonate habitability that is well preserved in the rock record. In contrast, the low observed Triassic habitability

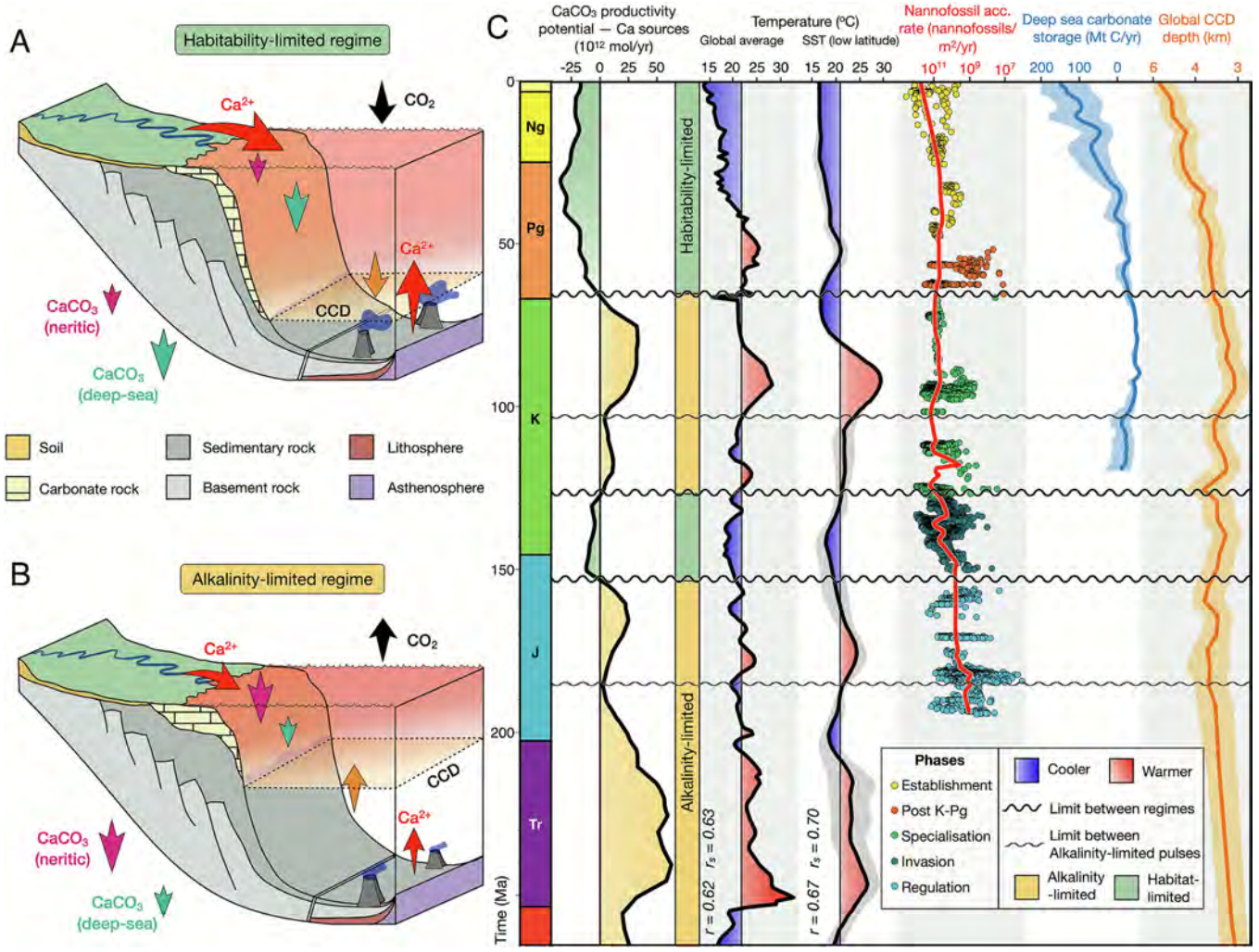

Fig. 4. Habitability- and alkalinity-limited regimes and implications on the carbonate compensation depth and Meso-Cenozoic climate regulation. (*A*) Habitability-limited regime. When neritic habitats are restricted, calcium ions saturate the water column, the carbonate compensation depth (CCD) deepens, and carbonate precipitation increases in deep waters. This regime is associated with enhanced deep-sea carbonate burial and relative atmospheric CO_2 drawdown. (*B*) Alkalinity-limited regime. When weathering and hydrothermal alkalinity inputs are low, carbonate ion availability becomes the limiting factor. Neritic precipitation depletes alkalinity, the CCD shoals, and deep-sea carbonates dissolve, weakening ocean buffering and allowing transient atmospheric CO_2 buildup. (*C*) Habitability-limited and alkalinity-limited regimes (green and orange, respectively) identified by the habitability excess, i.e., the difference between the maximum productivity potential of shallow-water carbonates and the Ca^{2+} and HCO_3^- influx. Habitability-limited and alkalinity-limited regimes match cooler-than-average and warmer-than-average periods of time, and habitability excess correlates to global average atmospheric (64) and low latitude sea surface (65) temperatures (Pearson (r) and Spearman (r_s) correlation coefficients of 0.6 to 0.7). Compiled nannofossil accumulation rates and associated LOESS curve [smoothing factor of 0.1, (74)] highlight several phases of calcifying pelagic algae evolutionary dynamic matching habitability-limited and alkalinity-limited regimes. Deep-sea sedimentary carbonate carbon storage since the Early Cretaceous (120 Ma to present) (5) and modeled global CCD (61). Triassic (Tr), Jurassic (J), Cretaceous (K), Paleogene (Pg), and Neogene (Ng).

is mainly due to a preservation bias, as only ~40% of modeled suitable areas remain at the surface of the Earth.

Shallow-Water Carbonate Productivity Through Time

Habitability sets the stage for shallow-water carbonate production but does not alone determine it. In other words, suitable habitat areas define where neritic carbonates could exist, but productivity—a mass per unit time—depends on how much carbonate actually accumulates. We next quantify the alkalinity-limited regime by estimating how ion supply and accommodation constrained carbonate accumulation. To translate suitable areas into carbonate productivity, we estimate deposition using stratigraphic accumulation rates. This yields the past productivity potential of warm-water carbonates. Because average accumulation rates inferred from deep-time records are orders of magnitude lower than modern rates and likely underestimate actual deposition (14, 37, 49), we use maximum accumulation rates (15) to provide an upper bound on productivity potential (*SI Appendix*). Productivity potential peaked during the Triassic (~8 Gt/y $CaCO_3$), the Late Jurassic (~5 Gt/y), and the Cretaceous (~7 Gt/y) (maximum productivity potential, Fig. 3*B* and *SI Appendix*, Fig. S6*B*), and reached the lowest values at the Eocene–Oligocene transition and ~2 Gt/yr in the Quaternary. These estimates may be inflated since carbonate accumulation also depends on accommodation space, which is controlled by shelf depth and sea-level (14, 49). For example, passive margins and rimmed platforms respond differently to sea-level changes, affecting the balance between potential and realized productivity (15, 16, 18). To bracket the plausible range of potential productivity, we also consider an alternative,

depth-limited scenario, in which deposition is capped by reconstructed paleo-shelf depths (22, 45). This provides a conservative lower bound (*SI Appendix*, Fig. S6 *A* and *B*; yellow lines), that likely underestimates actual accumulation since it does not include subsidence or compaction.

A more serious limitation is the availability of dissolved ions—Ca^{2+} and HCO_3^-—necessary for carbonate precipitation (*SI Appendix*, Fig. S6*C*). Our maximum estimates assume unlimited supply, yet ion inputs varied over time. To account for chemical constraints, we scale riverine fluxes to sediment and water discharge (24), and hydrothermal fluxes to mid-ocean ridge length and spreading rates (50). Although it inevitably involves uncertainties due to limited constraints on reconstructed past fluxes, this provides a first-order constraint on productivity (Fig. 3*B* and *SI Appendix*, Fig. S6*C*), adequate for capturing long-term trends rather than precise values.

Curbing the predicted productivity with these constraints, it follows that Triassic and Jurassic productivity would have been chemically limited to 25% of its potential, due to riverine fluxes two to four times lower than today (24) (Fig. 3 *B* and *C*). In contrast, a mid-Cretaceous (125 to 100 Ma) maximum of 4.2 Gt/y reflects high riverine inputs, ridge length, and spreading rates following the breakup of Pangea (50), and widespread habitat availability (Figs. 2 and 3*A*). Enhanced pelagic carbonate fluxes during the Early Cretaceous, as documented from nannofossil records (51), further support the view that neritic-pelagic partitioning strongly influenced global carbonate burial during this interval. During the Cenozoic, productivity declined due to mid-ocean ridge subduction, reduced hydrothermal fluxes, and the contraction of warm-water subtropics associated with long-term climate cooling, all of which restricted neritic habitability (50). Taken together, our results indicate that shallow-water carbonate productivity was shaped by three dominant drivers through time: i) weathering and riverine fluxes during the Triassic and Jurassic, ii) geodynamic activity and hydrothermal inputs during the Late Cretaceous, and iii) neritic habitat extent during the Early Cretaceous and Cenozoic.

In general, when chemical limits are applied together with habitability forcings, our productivity estimates converge with previous models for the Cretaceous (37) and also align with observational estimates for the Paleogene and Neogene (5) (Fig. 3*C*). While our estimates exceed field-based observations for the Cretaceous (5, 52), this reflects differences in spatial coverage: field data are restricted to the Tethyan realm (52) or preserved carbonate platforms (5), whereas our model predicts a more extensive global distribution of suitable environments (Fig. 1 and *SI Appendix*, Fig. S2*B*).

Warm-Water Carbonates as Modulators of Ocean Chemistry and Recovery Timescales

Chemical fluxes and neritic habitability regulate oceanic Ca^{2+} and HCO_3^- concentrations, with potentially far-reaching implications for atmospheric pCO_2 (18, 53–55). When neritic habitability is limited, calcium and alkalinity build up in the global ocean reservoir, increasing saturation states and leading to a deepening of both carbonate compensation depth (CCD, here and throughout this term is used in a broad sense to encompass both the calcite and aragonite compensation depths) and lysocline (56). Under these conditions, carbonate precipitation shifts to the deep ocean, promoting pelagic carbonate accumulation (Fig. 4*A*). Based on our predicted productivity trends (Fig. 3*C*), this habitability-limited regime intensified during the Paleogene—peaking around the Eocene–Oligocene transition—and also characterized parts of the Early Cretaceous (Fig. 4*C*). Conversely, during intervals when hydrothermal and riverine inputs of Ca^{2+} and HCO_3^- are low, oceanic ion concentrations are depleted by efficient uptake into shallow-water carbonates. In this alkalinity-limited regime, carbonate precipitation is restricted to neritic environments, and the CCD and lysocline lie at shallow depths (Fig. 4*B*). This regime dominates during the Triassic, Middle Jurassic, and Late Cretaceous, reflecting periods of limited chemical influx.

In the habitability-limited regime, elevated calcium concentrations, increased seawater alkalinity and pH, and a deepened CCD collectively enhance the efficiency of the carbonate pump. This state corresponds to the Cretan Ocean mode, characterized by low carbonate saturation and dominated by biogenic pelagic $CaCO_3$ precipitation (54). In contrast, the alkalinity-limited regime is marked by a shallow CCD and dissolved deep-water carbonates. This mode aligns with the Neritan Ocean, where $CaCO_3$ saturation is controlled by biogenic shallow-water carbonate precipitation (54). As proposed by Zeebe and Westbroek (54), both modes exert a significant influence on ocean carbonate chemistry and atmospheric pCO_2, thereby modulating global surface temperatures over geologic time. We propose that the alternation between habitability-limited and alkalinity-limited regimes, and their $CaCO_3$ saturation states, is not merely a mechanism for shifting the locus of carbonate deposition between shelves and the deep sea. Instead, it represents a fundamental regulatory process that modulates Earth's climate on 10^3-10^5 year timescales, by shaping recovery from perturbations, while interacting with slower 10^5 to 10^6 y silicate weathering feedbacks (54).

A key implication of this framework is that neritic carbonates modulate the recovery timescales of the carbon cycle (10^3 to 10^5 y). Carbonate burial can occur either in shallow-water (neritic) platforms or in the deep ocean (pelagic) and both systems are tightly coupled through their shared influence on the ocean's alkalinity balance and saturation state. Accumulation of $CaCO_3$ on continental shelves draws down alkalinity from surface waters, lowering carbonate ion concentration and surface saturation, which in turn decreases pelagic carbonate production and shoals the compensation depth. Conversely, efficient export of pelagic $CaCO_3$ to the deep ocean also reduces surface saturation, potentially limiting neritic precipitation. Thus, neither shallow- nor deep-water carbonate deposition is the sole driver of global carbonate burial; rather, they are in a dynamic equilibrium that governs ocean buffering and long-term CO_2 regulation (46, 57). Pelagic carbonate burial provides a globally integrated buffering mechanism: if atmospheric CO_2 rises, enhanced dissolution deepens the CCD until balance is restored. Neritic burial, by contrast, is spatially patchy, episodic, and sensitive to sea level and ecology, making the system less flexible. In neritic-dominated intervals, perturbations such as volcanic CO_2 release or enhanced weathering fluxes take longer to neutralize. This partitioning does not alter the ultimate CO_2 balance, which is set by silicate weathering on 10^5 to 10^6 y timescales, but it does shape the intermediate recovery window: pelagic-dominated states—the Cretan mode of Zeebe and Westbroek (54)—shorten recovery to tens of thousands of years, whereas neritic-dominated states—the Neritan mode (54)—prolong perturbations into the 10^5 y range (58–60).

Estimates of past atmospheric pCO_2 (39, 53) remain too uncertain to directly validate our hypothesis. Nonetheless, previously observed trends—such as the variability in the carbonate compensation depth (CCD) and deep-water carbonate accumulation

during the Paleogene—are broadly consistent with our proposed framework (5, 61) (Fig. 4*C*). In particular, the CCD was relatively deep in the Paleocene but shoaled markedly during the Early to Mid Eocene greenhouse before deepening again in the Oligocene (62, 63), a pattern that parallels long-term Cenozoic cooling and changing carbonate burial regimes. However, only the most recent habitability-limited interval is well documented (4, 5, 61), making deeper-time validation difficult. Support for our hypothesis comes from the habitability excess—defined as the difference between the potential productivity of shallow-water carbonates (Fig. 3*B*) and the estimated chemical influx. This excess closely tracks global mean atmospheric temperatures (64) and low-latitude sea surface temperatures (65) (Fig. 4*C*, Pearson and Spearman correlation coefficients > 0.6). Periods of habitability limitation correspond to cooler-than-average climatic phases—such as the Early Cretaceous and the Late Paleogene to Neogene—whereas alkalinity-limited regimes align with warmer-than-average intervals, including the Triassic, Middle and Late Jurassic, and the Cretaceous (Fig. 4*C*). These polarity matches hold true 72% of the time for the global mean temperature and 86% for sea surface temperature. One might argue that habitability is itself dependent on temperature, and therefore on pCO_2, potentially introducing a circular logic. However, our results show that this is unlikely: habitability is largely insensitive to pCO_2 variations in the climate simulations (Fig. 2*B* and *SI Appendix*, Fig. S3) and that neither the potential nor the actual productivity curves resemble the global mean (64) or tropical sea surface temperatures (65). This decoupling rules out circular reasoning.

As carbonate precipitation and dissolution respond sensitively to saturation state and climate feedback (66), the system self-adjusts and modulates Earth's climate and carbon cycle (54). In alkalinity-limited conditions, the ocean's buffering effect is hampered by low saturation and low pelagic productivity, which in turn could increase atmospheric pCO_2 (and conversely in habitability-limited conditions), while keeping the fluxes balanced between surficial and carbonate rock reservoirs, i.e., a succession of dynamic equilibrium that prevail as long as the boundary conditions—here set by habitability and fluxes—remain unchanged. However, the timescale of this feedback mechanism is thus critical, and additional constraints from carbon cycle modeling are essential to disentangle the causal relationships linking carbonate deposition regimes, ocean chemistry and climate, and in fine to quantify the impact of habitability- and alkalinity-limited regimes on long-term carbon cycling (60, 66, 67). A comprehensive evaluation should integrate the interactions between alkalinity, dissolved inorganic carbon, pH, lysocline and CCDs (68, 69), calcite saturation state, Mg/Ca ratios, organic matter burial, and biological pumping (46). For example, during the Mesozoic—particularly in the Triassic, Middle Jurassic, and Middle Cretaceous—global warming and elevated atmospheric pCO_2 likely intensified silicate weathering (24), especially in tectonically active and humid tropical regions. In this process, atmospheric CO_2 reacts with silicate minerals to produce bicarbonate ions that are transported to the oceans, raising alkalinity. This, in turn, improves the buffering capacity of the ocean against CO_2, increases and promotes carbonate precipitation, and contributes to long-term carbon sequestration (67, 70, 71). The silicate weathering feedback serves as one of several critical negative feedbacks that moderate extreme fluctuations in pCO_2 (3), ultimately helping to stabilize the climate by regulating marine carbonate deposition (72, 73). Among the many interactions, we identified two of them that depend on the alternation between habitat-limited and alkalinity-limited regions and that could have profound consequences for marine life and climate.

First, warm-water carbonate habitability modulates, among other factors, nutrient delivery to the oceans, with potentially profound consequences for marine biodiversification (24). Calcium and alkalinity are crucial to pelagic calcifiers, which in turn contribute to set the carbonate regimes at play (54). The rise of pelagic calcifiers during the Meso-Cenozoic period (46) is therefore particularly relevant: nannofossil accumulation rates show phases of variability—alternating increases and stasis—rather than a long-term monotonic trend (74) (Fig. 4*C*); these fluctuations align with our predicted shifts in carbonate regimes and provide a framework to reinterpret the underlying evolutionary controls. During the Triassic and Jurassic, a prolonged alkalinity-limited, Neritan regime restricted terrestrial fluxes to the oceans (54), inhibiting the development of pelagic calcifiers. During this "regulation-phase" (74) their productivity was therefore too low to accumulate and fossilize as rock units. In contrast, the habitability-limited, Cretan interval spanning the Upper Jurassic to Lower Cretaceous promoted nutrient export to the open ocean, triggering a phase of nannoplankton expansion. A subsequent return to alkalinity-limited, Neritan conditions through the remainder of the Cretaceous coincides with a phase of stasis (or even slight decline) in nannofossil accumulation and the onset of a specialization phase, potentially driven by increased environmental stress—specifically, nutrient limitation from reduced terrestrial inputs. Following the K-Pg extinction, nannofossil accumulation rates increased markedly from the Eocene to the Neogene, corresponding to platform progradation and a renewed phase of nannoplankton expansion consistent with the ultimate habitability-limited, Cretan phase. These processes act together with other biotic factors that introduced evolutionary innovations and additional ecological complexity. For example, the diversification of foraminifera and diatoms that reshaped the pelagic food webs and the cycling of nutrients during the Cretaceous and through the Neogene (75, 76), as well as the evolutionary constraints that limited the ecological niche of nannoplankton until the later Jurassic (8), probably contributed to the development of pelagic calcifiers. While the alignment of these evolutionary phases with our carbonate regimes is striking, further geochemical validation is required to confirm the link between nutrient fluxes and biotic evolution. This evolution highlights that across the Meso-Cenozoic, alternation between habitability-limited and alkalinity-limited regimes did not correspond to a simple switch between low and high nannofossil accumulation rates. Instead, these intervals reflect dynamic phases of "regulation, invasion, specialization, and establishment" of pelagic calcifiers (74). As a result, while the partitioning of carbonate burial between neritic and pelagic environments influenced the ecological expansion of nannoplankton, the rise and diversification of these pelagic calcifiers also progressively modified the biological pump and feedbacks within the carbon cycle.

Second, neritic carbonates also indirectly modulate the pelagic carbonate pump and the organic carbon cycle. Expanded neritic platforms enhance nutrient leakage to the open ocean, stimulating pelagic productivity and reinforcing the efficiency of the carbonate pump (46, 54). At the same time, increased nutrient delivery promotes organic carbon burial in marine sediments, providing an additional sink for atmospheric CO_2 (77, 78). This link implies that shifts in neritic habitability not only affected carbonate deposition partitioning but also the balance

between silicate weathering and organic carbon burial in the long-term carbon cycle. In steady state, the carbon budget can be expressed as CO_2 outgassing plus kerogen weathering balanced by silicate weathering plus organic carbon burial (3, 79). By modulating nutrient fluxes, neritic carbonates could therefore influence the silicate weathering "set-point": higher rates of organic carbon burial would reduce the required silicate weathering flux, potentially leading to lower atmospheric pCO_2 and cooler climates. This feedback highlights a more complex interplay between carbonate deposition, nutrient dynamics, and the regulation of steady-state CO_2 than previously considered, with implications for both the evolution of pelagic calcifiers and the coupling of inorganic and organic carbon cycles across the Meso-Cenozoic. Moreover, the expansion of nannoplankton—and biotic carbonate precipitation more broadly—may itself represent an important feedback in the global carbon cycle. Incorporating this biological component into future carbon cycle models could improve reconstructions of past atmospheric pCO_2 and temperature dynamics.

Carbonate burial is a well-identified regulator of Earth's climate (60, 66), but our study refines this view by identifying two alternating regimes—habitability-limited and alkalinity-limited—that structured the Meso-Cenozoic carbon cycle. We show that weathering and geodynamic fluxes, together with neritic habitability, controlled the partitioning of carbonate deposition between shallow-water platforms and the deep ocean. This partitioning not only established the locus of long-term carbonate sequestration but also modulated the efficiency of ocean buffering, thus regulating the recovery timescales of the carbon cycle (10^3 to 10^5 y). Pelagic-dominated burial improved buffering and allowed faster recovery from CO_2 perturbations, whereas neritic-dominated burial reduced buffering capacity, prolonging climatic impacts until silicate weathering restored balance on multimillion-year timescales (58, 59).

This sink-focused perspective complements source-driven explanations of long-term climate change and helps reconcile major transitions: for example, Cenozoic cooling linked to enhanced pelagic burial (4–6), and Quaternary fluctuations tied to shallow-water productivity (31, 80, 81). Our framework also offers a lens on biotic evolution, suggesting that regime shifts interacted with ecology and competition and influenced the diversification of pelagic calcifiers, culminating in the Neogene dominance of coccolithophores (74), in line with broader patterns of evolution and diversity of calcareous nannoplankton (8, 82).

By combining geodynamic, climatic, and physiographic reconstructions with macroecological simulations, we provide continuous reconstructions of neritic habitability and productivity over the past 265 My. Together, these results confirm our central hypothesis: Earth's long-term carbon cycle oscillated between habitability-limited and alkalinity-limited states, with the transition between them governing how efficiently the ocean buffered climatic perturbations. Produced datasets go beyond the spatial and temporal gaps of the fossil record and open the way to more quantitative assessments of the coupled evolution of carbonate deposition, atmospheric CO_2, and biodiversity.

Materials and Methods

We integrated global reconstructions of plate tectonics and paleogeography (22, 45), climate simulations from the HadCM3BL-M2.1aD model (23), and modeled sediment fluxes from the goSPL landscape evolution model (24, 83) to explore the evolution of warm-water carbonate systems over the past 265 My. Environmental variables including sea surface temperature, salinity, ocean currents, shelf extent, and sediment input were extracted, regridded at 0.1° resolution, and used to build species distribution models (SDMs) with the Biomod2 package (25, 84, 85). These SDMs estimate the distribution of suitable habitats by linking modern carbonate occurrences (12) to environmental parameters and were evaluated through cross-validation and comparison with the PaleoReef fossil database (29). Predicted habitat areas were combined with published carbonate accumulation rates (14, 15) and estimates of calcium and alkalinity flux from weathering, groundwater, and hydrothermal inputs (18, 86–89) to reconstruct carbonate productivity and carbon sequestration potential through time.

Data, Materials, and Software Availability. Paleo-environmental oceanic variables are available from the BRIDGE website: https://www.paleo.bristol.ac.uk. The paleo-coastlines dataset is compiled in a Zenodo repository: https://doi.org/10.5281/zenodo.3903163. Sediment flux from the global-scale landscape evolution is available from HydroShare (90). The scientific software used in this study, BIOMOD2, can be found in https://biomodhub.github.io/biomod2. Our simulation inputs and outputs (ensemble models) are available from Zenodo (https://doi.org/10.5281/zenodo.10073627). R and Python scripts as well as the Jupyter notebooks used in our pre- and postprocessing workflows are available from the following GitHub link: https://github.com/Geodels/paleoReef. Sediment flux is available from HydroShare (https://www.hydroshare.org/resource/0106c156507c4861b4cfd404022f9580/).

ACKNOWLEDGMENTS. This research was carried out with resources from the National Computational Infrastructure supported by the Australian Government and Artemis HPC supported by the University of Sydney. This work was primarily supported by Australian Research Council grants IC190100031 and DP220101125. We thank anonymous reviewers and the editor for their constructive and thoughtful feedback, which greatly improved the clarity, balance, and impact of this manuscript.

Author affiliations: [a]School of Geosciences, University of Sydney, Camperdown, NSW 2006, Australia; [b]Université Grenoble Alpes, Institut des Sciences de la Terre, Centre National de la Recherche Scientifique, Grenoble 38000, France; and [c]Geocoastal Research Group, School of Geosciences, University of Sydney, Camperdown, NSW 2006, Australia

Author contributions: T.S. designed research; T.S. and L.H. performed research; T.S. and T.T.N. contributed new reagents/analytic tools; T.S., L.H., T.T.N., A.V.-C., J.L., A.P.D.S., J.M.W., and F.G. analyzed data; and T.S., L.H., A.V.-C., J.L., A.P.D.S., J.M.W., and F.G. wrote the paper.

1. R. A. Berner, A. C. Lasaga, R. M. Garrels, The carbonate-silicate geochemical cycle and its effect on atmospheric carbon dioxide over the past 100 million years. *Am. J. Sci.* **283**, 641–683 (1983).
2. L. R. Kump, M. A. Arthur, Interpreting carbon-isotope excursions: Carbonates and organic matter. *Chem. Geol.* **90**, 1–10 (1991).
3. R. A. Berner, K. Caldeira, The need for mass balance and feedback in the geochemical carbon cycle. *Geology* **25**, 955–956 (1997).
4. B. N. Opdyke, B. H. Wilkinson, Surface area control of shallow cratonic to deep marine carbonate accumulation. *Paleoceanography* **3**, 685–703 (1988).
5. A. Dutkiewicz, D. Müller, J. Cannon, S. Vaughan, S. Zahirovic, Sequestration and subduction of deep-sea carbonate in the global ocean since the Early Cretaceous. *Geology* **47**, 91–94 (2019).
6. M. Bogumil, T. Mittal, C. Lithgow-Bertelloni, The effects of bathymetry on the long-term carbon cycle and CCD. *Proc. Natl. Acad. Sci. U.S.A.* **121**, e2400232121 (2024).
7. W. H. Berger, E. L. Winterer, *Plate Stratigraphy and the Fluctuating Carbonate Line* (IAS Special Publications, 1981), vol. 1.
8. P. G. Falkowski *et al.*, The evolution of modern eukaryotic phytoplankton. *Science* **305**, 354–360 (2004).
9. A. Hilting, L. R. Kump, T. J. Bralower, Variations in the oceanic vertical isotope gradient and their implications for the oceanic carbon cycle. *Paleoceanogr. Paleoclimatol.* **23**, PA4214 (2008).
10. W. Schlager, Benthic carbonate factories of the Phanerozoic. *Int. J. Earth Sci.* **92**, 445–464 (2003).
11. J. Michel *et al.*, Marine carbonate factories: A global model of carbonate platform distribution. *Int. J. Earth Sci.* **108**, 1773–1792 (2019).
12. M. Laugié, J. Michel, A. Pohl, E. Poli, J. Borgomano, Global distribution of modern shallow-water marine carbonate factories: A spatial model based on environmental parameters. *Sci. Rep.* **9**, 16432 (2019).
13. J. J. G. Reijmer, Marine carbonate factories: Review and update. *Sedimentology* **68**, 1729–1796 (2021).
14. H. Bosscher, W. Schlager, Accumulation rates of carbonate platforms. *J. Geol.* **101**, 345–355 (1993).

15. W. Kiessling, E. Flügel, J. Golonka, Patterns of Phanerozoic carbonate platform sedimentation. *Lethaia* **36**, 195–225 (2003).
16. W. Kiessling, Long-term relationships between ecological stability and biodiversity in Phanerozoic reefs. *Nature* **433**, 410–413 (2005).
17. J. Wilson, *Carbonate Facies in Geologic History* (Springer, Berlin/Heidelberg, Germany, 1975).
18. S. M. Stanley, L. A. Hardie, Secular oscillations in the carbonate mineralogy of reef-building and sediment-producing organisms driven by tectonically forced shifts in seawater chemistry. *Palaeogeogr., Palaeoclimatol., Palaeoecol.* **144**, 3–19 (1998).
19. W. Renema *et al*., Hopping hotspots: Global shifts in marine biodiversity. *Science* **321**, 654–657 (2008).
20. T. Steuber, H. Löser, J. Mutterlose, M. Parente, Biogeodynamics of Cretaceous marine carbonate production. *Earth-Sci. Rev.* **238**, 104341 (2023).
21. A. Tassy *et al*., Global geodynamic control on Phanerozoic marine carbonates sedimentary systems. *Lithosphere* **2023**, 9689299 (2023).
22. A. Kocsis, C. Scotese, Mapping paleocoastlines and continental flooding during the Phanerozoic. *Earth Sci. Rev.* **213**, 103463 (2021).
23. P. Valdes, C. Scotese, D. Lunt, Deep ocean temperatures through time. *Clim. Past* **17**, 1483–1506 (2021).
24. T. Salles, L. Husson, M. Lorcery, B. H. Boggiani, Landscape dynamics and the Phanerozoic diversification of the biosphere. *Nature* **624**, 115–121 (2023).
25. M. Guéguen, H. Blancheteau, W. Thuiller, biomod2: Ensemble platform for species distribution modeling. R package (Version 4.3-4, R. package, 2025), https://biomodhub.github.io/biomod2/.
26. E. Couce, A. Ridgwell, E. J. Hendy, Environmental controls on the global distribution of shallow-water coral reefs. *J. Biogeogr.* **39**, 1508–1523 (2012).
27. L. Jones, P. Mannion, A. Farnsworth, F. Bragg, D. Lunt, Climatic and tectonic drivers shaped the tropical distribution of coral reefs. *Nat. Commun.* **13**, 1–10 (2022).
28. A. Ziegler, M. Hulver, A. Lottes, W. Schmachtenberg, Uniformitarianism and palaeoclimates: Inferences from the distribution of carbonate rocks. *Fossils Clim.* **11**, 3–25 (1984).
29. W. Kiessling, C. Krause, PaleoReefs database (PARED) (2022). https://doi.org/10.5281/zenodo.6037852.
30. D. Jablonski, K. Roy, J. W. Valentine, R. M. Price, P. S. Anderson, The impact of the pull of the recent on the history of marine diversity. *Science* **300**, 1133–1135 (2003).
31. L. Husson *et al*., Reef carbonate productivity during quaternary sea level oscillations. *Geochem., Geophys., Geosyst.* **19**, 1148–1164 (2018).
32. M. Lorcery *et al*., Deep time evolution of the latitudinal diversity gradient: Insights from mechanistic models. *PLoS ONE* **20**, 1–21 (2025).
33. K. Miller *et al*., The Phanerozoic record of global sea-level change. *Science* **310**, 1293–1298 (2005).
34. D. Gröcke, G. Price, A. Ruffell, J. Mutterlose, E. Baraboshkin, Isotopic evidence for Late Jurassic-Early Cretaceous climate change. *Palaeogeogr., Palaeoclimatol., Palaeoecol.* **202**, 97–118 (2003).
35. J. Zachos, G. Dickens, R. Zeebe, An Early Cenozoic perspective on Greenhouse warming and carbon cycle dynamics. *Nature* **451**, 279–283 (2008).
36. M. Vickers *et al*., The duration and magnitude of Cretaceous cool events: Evidence from the northern high latitudes. *GSA Bull.* **131**, 1979–1994 (2019).
37. A. Pohl *et al*., Carbonate platform production during the Cretaceous. *GSA Bull.* **132**, 2606–2610 (2020).
38. P. Skelton, S. Sano, J. P. Masse, Rudist bivalves and the Pacific in the Late Jurassic and Early Cretaceous. *J. Geol. Soc.* **170**, 513–526 (2013).
39. G. Foster, D. Royer, D. Lunt, Future climate forcing potentially without precedent in the last 420 million years. *Nat. Commun.* **8**, 14845 (2017).
40. L. A. Jones, C. D. Dean, P. D. Mannion, A. Farnsworth, P. A. Allison, Spatial sampling heterogeneity limits the detectability of deep time latitudinal biodiversity gradients. *Proc. R. Soc. B Biol. Sci.* **288**, 20202762 (2021).
41. J. Crame, B. Rosen, Cenozoic palaeogeography and the rise of modern biodiversity patterns. *Geol. Soc., London, Spec. Publ.* **194**, 153–168 (2002).
42. F. Leprieur *et al*., Plate tectonics drive tropical reef biodiversity dynamics. *Nat. Commun.* **7**, 11461 (2016).
43. A. Pohl *et al*., Quantifying the paleogeographic driver of Cretaceous carbonate platform development using paleoecological niche modeling. *Palaeogeogr., Palaeoclimatol., Palaeoecol.* **514**, 222–232 (2019).
44. L. Walker, B. Wilkinson, L. Ivany, Continental drift and phanerozoic carbonate accumulation in shallow-shelf and deep-marine settings. *J. Geol.* **110**, 75–87 (2002).
45. C. Scotese, N. Wright, PALEOMAP paleodigital elevation models (PaleoDEMS) for the Phanerozoic (2018). https://doi.org/10.5281/zenodo.5460860.
46. A. Ridgwell, R. E. Zeebe, The role of the global carbonate cycle in the regulation and evolution of the earth system. *Earth Planet. Sci. Lett.* **234**, 299–315 (2005).
47. Z. Chen *et al*., *World Karst Aquifer Map (WHYMAP WOKAM)* (BGR/IAH/KIT/UNESCO, 2017).
48. C. Hoorn, F. P. Wesselingh, J. Hovikoski, J. Guerrero, *The Development of the Amazonian Mega-Wetland (Miocene, Brazil, Colombia, Peru, Bolivia)* (John Wiley & Sons, Ltd., 2009), pp. 123–142.
49. W. Schlager, Carbonate sedimentology and sequence stratigraphy. Concepts in sedimentology and paleontology. *Soc. Econ. Paleontol. Mineral.* **8**, 13–51 (2005).
50. D. Müller *et al*., Evolution of Earth's tectonic carbon conveyor belt. *Nature* **605**, 629–639 (2022).
51. E. Erba, F. Tremolada, Nannofossil carbonate fluxes during the Early Cretaceous: Phytoplankton response to nutrification episodes, atmospheric CO_2, and anoxia. *Paleoceanogr. Paleoclimatol.* **19**, PA1008 (2004).
52. P. Skelton, R. Spicer, S. Kelley, I. Gilmour, *The Operation of the Major Geological Carbon Sinks* (Cambridge University Press, 2003), pp. 259–266.
53. B. J. Mills *et al*., Modelling the long-term carbon cycle, atmospheric CO_2, and Earth surface temperature from late Neoproterozoic to present day. *Gondwana Res.* **67**, 172–186 (2019).
54. R. E. Zeebe, P. Westbroek, A simple model for the $CaCO_3$ saturation state of the ocean: The "Strangelove," the "Neritan," and the "Cretan" Ocean. *Geochem., Geophys., Geosyst.* **4**, 1104 (2003).
55. J. Ware, S. Smith, M. Reaka, Coral reefs: Sources or sinks of atmospheric CO_2? *Coral Reefs* **11**, 127–130 (1992).
56. L. R. Kump, M. A. Arthur, "Global chemical erosion during the Cenozoic: Weatherability balances the budgets" in *Tectonic Uplift and Climate Change*, W. F. Ruddiman, Ed. (Springer, 1997), pp. 399–426.
57. J. D. Milliman, Production and accumulation of calcium carbonate in the ocean: Budget of a nonsteady state. *Global Biogeochem. Cycles* **7**, 927–957 (1993).
58. N. S. Lord, A. Ridgwell, M. C. Thorne, D. J. Lunt, Biogeochemical impacts of phytoplankton community structure. *Global Biogeochem. Cycles* **29**, 456–476 (2015).
59. B. Hönisch *et al*., The geological record of ocean acidification. *Science* **335**, 1058–1063 (2012).
60. A. J. Ridgwell, An end to the "rain ratio" reign? *Geochem., Geophys., Geosyst.* **4**, 1051 (2003).
61. S. Boss, B. Wilkinson, Planktogenic/eustatic control on cratonic/oceanic carbonate accumulation. *J. Geol.* **99**, 497–513 (1991).
62. H. Pälike *et al*., A Cenozoic record of the equatorial Pacific carbonate compensation depth. *Nature* **488**, 609–614 (2012).
63. T. J. Bralower, Evidence of surface water oligotrophy during the Paleocene–Eocene thermal maximum: Nanofossil assemblage data from ocean drilling program site 690, maud rise. *Paleoceanography* **17**, 13-1–13-12 (2002).
64. C. R. Scotese, H. Song, B. J. Mills, D. G. van der Meer, Phanerozoic paleotemperatures: The earth's changing climate during the last 540 million years. *Earth Sci. Rev.* **215**, 103503 (2021).
65. H. Song, P. Wignall, H. Song, X. Dai, D. Chu, Seawater temperature and dissolved oxygen over the past 500 million years. *J. Earth Sci.* **30**, 236–243 (2019).
66. Y. Donnadieu *et al*., A mechanism for brief glacial episodes in the Mesozoic greenhouse. *Paleoceanography* **26**, PA3212 (2011).
67. R. A. Berner, Geocarb II: A revised model of atmospheric CO_2 over Phanerozoic time. *Am. J. Sci.* **294**, 56–91 (1994).
68. S. E. Greene *et al*., Early Cenozoic decoupling of climate and carbonate compensation depth trends. *Paleoceanogr. Paleoclimatol.* **34**, 930–945 (2019).
69. J. J. Middelburg, K. Soetaert, M. Hagens, Ocean alkalinity, buffering and biogeochemical processes. *Rev. Geophys.* **58**, e2019RG000681 (2020).
70. P. Raymond, J. Cole, Increase in the export of alkalinity from North America's largest river. *Science* **301**, 88–91 (2003).
71. R. Zeebe, K. Caldeira, Close mass balance of long-term carbon fluxes from ice-core CO_2 and ocean chemistry records. *Nat. Geosci.* **1**, 312–315 (2008).
72. M. E. Raymo, W. F. Ruddiman, Tectonic forcing of late Cenozoic climate. *Nature* **359**, 117–122 (1992).
73. A. Ridgwell, A Mid Mesozoic Revolution in the regulation of ocean chemistry. *Mar. Geol.* **217**, 339–357 (2005).
74. B. Suchéras-Marx *et al*., The colonization of the oceans by calcifying pelagic algae. *Biogeosciences* **16**, 2501–2510 (2019).
75. S. Westacott, N. J. Planavsky, M. Y. Zhao, P. M. Hull, Revisiting the sedimentary record of the rise of diatoms. *Proc. Natl. Acad. Sci. U.S.A.* **118**, e2103517118 (2021).
76. R. Morard *et al*., Renewal of planktonic foraminifera diversity after the Cretaceous Paleogene mass extinction by benthic colonizers. *Nat. Commun.* **13**, 1–9 (2022).
77. W. W. Hay, Carbonate fluxes and calcareous nannoplankton. *Geol. Soc., London, Spec. Publ.* **303**, 15–35 (2008).
78. S. Arndt, A. Ridgwell, L. Lourens, Biogeochemical models of marine carbon cycle perturbations: Limitations and perspectives. *Global Biogeochem. Cycles* **25**, GB2010 (2011).
79. L. R. Kump, M. A. Arthur, Interpreting carbon-isotope excursions: Carbonates and organic matter. *Chem. Geol.* **161**, 181–198 (1999).
80. W. Berger, Increase of carbon dioxide in the atmosphere during deglaciation: The coral reef hypothesis. *Naturwissenschaften* **69**, 87–88 (1982).
81. B. N. Opdyke, J. C. Walker, Return of the coral reef hypothesis: Basin to shelf partitioning of $CaCO_3$ and its effect on atmospheric CO_2. *Geology* **20**, 733–736 (1992).
82. P. R. Bown, J. A. Lees, J. R. Young, "Calcareous nannoplankton evolution and diversity through time" in *Coccolithophores: From Molecular Processes to Global Impact*, H. R. Thierstein, J. R. Young, Eds. (Springer, Berlin, Germany, 2004), pp. 481–508.
83. T. Salles, C. Mallard, S. Zahirovic, goSPL: Global scalable paleo landscape evolution. *J. Open Source Software* **5**, 2804 (2020).
84. W. Thuiller, B. Lafourcade, R. Engler, M. B. Araújo, BIOMOD–A platform for ensemble forecasting of species distributions. *Ecography* **32**, 369–373 (2009).
85. T. Hao, J. Elith, G. Guillera-Arroita, J. J. Lahoz-Monfort, A review of evidence about use and performance of species distribution modelling ensembles like BIOMOD. *Diversity Distrib.* **25**, 839–852 (2019).
86. J. Milliman, A. Droxler, Neritic and pelagic carbonate sedimentation in the marine environment: Ignorance is not bliss. *Geol. Rundsch.* **85**, 496–504 (1996).
87. J. Gaillardet, B. Dupré, P. Louvat, C. Allègre, Global silicate weathering and CO_2 consumption rates deduced from the chemistry of large rivers. *Chem. Geol.* **159**, 3–30 (1999).
88. M. Ligi, E. Bonatti, M. Cuffaro, D. Brunelli, Post-Mesozoic rapid increase of seawater Mg/Ca due to enhanced mantle-seawater interaction. *Sci. Rep.* **3**, 2752 (2013).
89. K. Mayfield *et al*., Groundwater discharge impacts marine isotope budgets of Li, Mg, Ca, Sr, and Ba. *Nat. Commun.* **12**, 148 (2021).
90. T. Salles, L. Husson, M. Lorcery, B. Halder Boggiani, Paleo-physiography project (2022). https://www.hydroshare.org/resource/0106c156507c4861b4cfd404022f9580 (Accessed 21 November 2025).